



Arterial Vehicle Trajectory Reconstruction Based on Stopbar Video Sensor for Automated Traffic Signal Performance Measures

Tianya Terry Zhang, Ph.D.¹; Peter J. Jin, Ph.D.²; Thomas M. Brennan Jr., Ph.D., P.E.³;
Kelly McVeigh⁴; Mohammad Jalayer, Ph.D.⁵; and Deep Patel⁶

Abstract: This paper addresses a key limitation of using existing detection and controller data of signalized intersections to build performance metrics in the automated traffic signal performance measures (ATSPMs) platform. Many intersections were installed with lane-by-lane stopbar detectors for actuated and adaptive signal controllers. Stopbar detector actuations are valuable inputs for signal controllers and intersection performance but are not the ideal advanced detector inputs for several key ATSPM metrics such as arrival on red (AoR) and Purdue coordination diagram (PCD). This paper presents a vehicle trajectory reconstruction algorithm based on shockwave theory to estimate advanced vehicle detections from stopbar arrivals and departures. Model parameters including shockwave speeds, free-flow velocity, acceleration, and deceleration rates were directly measured using spatial-temporal maps (STMaps) generated from roadside closed-circuit television (CCTV) camera video. The initially measured parameters were optimized using the genetic algorithm (GA) that was subsequently validated quantitatively and qualitatively. Finally, combining the stopbar detector and signal phase and timing, a new coordination diagram was designed to enable traffic operators to identify mobility patterns and safety-critical events quickly. This research sought to utilize existing data sources to meet performance metric requirements while avoiding intensive investment to upgrade the current infrastructure. The STMap-based method substantially reduces the complexity of obtaining necessary model parameters. The new stopbar-based Rutgers coordination diagram enriches the visualization tools for intersection performance measures from controller and detection systems. DOI: [10.1061/JTEPBS.0000749](https://doi.org/10.1061/JTEPBS.0000749).

© 2023 American Society of Civil Engineers.

Author keywords: Signal performance measures; Stopbar detector; Closed-circuit television (CCTV) camera.

Introduction

Reducing delay while improving capacity and safety are key traffic operation and maintenance goals. A well-timed traffic signal can significantly decrease waiting delay, reduce the crash frequency, and increase traffic throughput. However, more than 50% of motor vehicle crashes, including injury and fatal crashes, occur at or

nearby an intersection according to Federal Highway Administration (FHWA) intersection safety and design research (FHWA 2021). To meet these mobility and safety goals, agencies need to obtain accurate traffic parameters and assess the effectiveness of the timing of a signalized corridor. Many conventional measures [e.g., *Highway Capacity Manual* (Manual 2010) and software-based simulation and optimization] rely on field data that are postprocessed to determine the effectiveness of a traffic signal system (e.g., delay, stops, and fuel consumption). This data collection often incurs high labor costs, restricting field studies to a specific scope and periods.

Conversely, a centrally managed real-time signal performance platform [e.g., automated traffic signal performance measures (ATSPMs)] provides a visualization tool for traffic engineers to evaluate both the real-time and historical functionality of signalized intersections. These near-real-time observations lead to proactively managed signalized corridors that can be quickly analyzed to minimize traffic delay, improve safety and travel time reliability, and save fuel costs through better-informed decision making. Unlike adaptive traffic signal control systems that were built with their own detection systems, ATSPMs, as a data-intensive application, mainly rely on existing detectors to collect vehicle actuation data. However, many agencies installed their detection systems not just for signalized intersections but also for the entire corridor/link monitoring. The traffic management center often faces the issue that it needs to upgrade its infrastructure to meet the data needs of ATSPMs, which incurs considerable amounts of investment. To avoid extra capital spending, the research tries to meet the data demands of ATSPMs with existing detection and controller data sources. More specifically, this paper developed a new methodology of using the lane-by-lane stopbar detector data and cycle-by-cycle

¹Ph.D. Candidate, Dept. of Civil and Environmental Engineering, Rutgers, State Univ. of New Jersey, 500 Bartholomew Rd., Room 420A, Piscataway, NJ 08854-8099 (corresponding author). ORCID: <https://orcid.org/0000-0002-7606-9886>. Email: tz140@scarletmail.rutgers.edu

²Associate Professor, Dept. of Civil and Environmental Engineering, Rutgers, State Univ. of New Jersey, 500 Bartholomew Rd., Room 420F, Piscataway, NJ 08854-8099. ORCID: <https://orcid.org/0000-0002-7688-3730>. Email: peter.j.jin@rutgers.edu

³Professor, Dept. of Civil Engineering, College of New Jersey, Armstrong Hall, RM 173, 2000 Pennington Rd., Ewing Township, NJ 08628. ORCID: <https://orcid.org/0000-0003-2316-4983>. Email: brennant@tcnj.edu

⁴Supervising Highway Engineer, Arterial Mobility Management, Transportation Operations Systems and Support, 1035 Parkway Ave., Trenton, NJ 08625. Email: Kelly.mcveigh@dot.nj.gov

⁵Associate Professor, Dept. of Civil and Environmental Engineering, Rowan Univ., 201 Mullica Hill Rd., Glassboro, NJ 08028. Email: jalayer@rowan.edu

⁶Graduate Research Assistant, Dept. of Civil and Environmental Engineering, Rowan Univ., 201 Mullica Hill Rd., Glassboro, NJ 08028. ORCID: <https://orcid.org/0000-0001-7595-7489>. Email: pateld80@rowan.edu

Note. This manuscript was submitted on October 29, 2021; approved on June 21, 2022; published online on January 27, 2023. Discussion period open until June 27, 2023; separate discussions must be submitted for individual papers. This paper is part of the *Journal of Transportation Engineering, Part A: Systems*, © ASCE, ISSN 2473-2907.

signal timing data to generate advanced detection events required by ATSPMs. In this research, we built an interface between the Sydney coordinated adaptive traffic system (SCATS) and ATSPMs to allow SCATS signal events and detection data to be directly ingested into ATSPMs database; the successful story of this attempt suggests that ATSPMs could evolve toward adaptive signal control system with real-time communication and computation, as discussed by Stevanovic (2020).

In previous research, Zhang et al. (2021a) developed a signal event converter to ingest SCATS and InSync controller history log files into ATSPMs and created signal controller performances. In a continuation of that previous work, this paper utilized a commonly installed stopbar detector to estimate vehicle arrivals at the advanced detector location. The effect of this method was validated on a selected key corridor, US-1 in New Jersey, equipped with a SCATS system, which is known for its continuous and autonomous measurement and self-calibration. The signal controller historical file and Autoscope (Image Sensing Systems, Minneapolis, Minnesota) detection records at Harrison intersection were collected from the New Jersey Department of Transportation (NJDOT) Arterial Management Center. This testing intersection is also covered by a closed-circuit television (CCTV) camera from the NJ511 system, which can provide video recordings for validating the reconstructed trajectory. The proposed method expands the capability of traditional video stopbar detector data to estimate the queuing process and reconstruct accurate vehicle trajectories at signalized intersections.

Relevant Work

Signal Performance Measures

Monitoring signal performance in real-time is challenging, requiring immediate data collection, processing, and analysis capabilities. To address the inefficient traffic signal optimization process, ATSPMs, a suite of performance measures and analysis tools, were promoted by FHWA's Every-Day Counts Round 4 (EDC-4) initiative. ATSPM-based systems are a context-sensitive and data-driven approach to arterial traffic management; they are considered revolutionary for traffic safety and mobility operation. In 2005, the Indiana Department of Transportation (INDOT) developed new traffic signal system performance measurements using logged timestamped vehicle detectors and high-resolution data. The Purdue coordination diagram (PCD) was introduced as a tool for visualizing and evaluating signal performances on a cycle-by-cycle basis, enabling the visual inspection of the concurrence of vehicle platoons within green bands (Day et al. 2008).

Day et al. (2012) tested the effectiveness of performance measures for adaptive signal control using system-in-the-loop simulation. The two objectives of signal control, allocating capacity to competing movements and traffic progression along corridors, were examined using two performance measurements created from high-resolution controller events. Remias et al. (2018a) evaluated four different types of vehicle detection data, including advanced detector data, Bluetooth/Wi-Fi sensors, segment-based probe vehicle data, and global positioning system (GPS)-based vehicle trajectories for coordinated intersections. All data sources can be used for problem identification, but the advanced detector and GPS data can reveal better coordination issues. Michigan DOT estimated an approximate 25:1 benefit-cost ratio for using ATSPMs through pilot testing by considering travel time reduction, emission reduction, safety benefits, maintenance, and operational benefits (Remias et al. 2018b). North Carolina DOT (Kimley-Horn 2019)

created an implementation matrix to prioritize corridors to implement ATSPMs, considering the possible levels of ATSPMs implementation.

Four factors affecting the readiness of deploying ATSPMs include central signal control, field hardware, ATSPMs software, and detection. Traffic operators familiar with ATSPMs have identified several shortcomings, such as a lack of data quality control and the intensive resources needed for systemwide management. An intelligent traffic signal performance measurement tool (ITSPM) was created to provide data quality control for ATSPMs and support data-driven traffic monitoring. The proposed ITSPM employs a machine learning method, traffic flow theory, and visualization to improve the state of the art (Huang et al. 2018).

Shockwave at Signalized Intersection

Shockwave theory has been used widely to capture the change of traffic state, where the traffic state is described by density, flow, and density, according to Lighthill-Whitham-Richards (LWR) traffic flow model (Lighthill and Whitham 1955). Geroliminis and Skabardonis (2005) applied the Markov decision process (MDP) to estimate traffic between continuous traffic signals. The shockwave theory was used for modeling traffic dynamics. Sharma et al. (2007) developed the input-output model and hybrid techniques to estimate queue length and delay at signalized intersections. The hybrid model takes advanced detector actuation, stopbar detector actuation, signal timing, and parametric data. The input-output model uses advanced detector actuation, phase-change data, and parametric data (saturation headway, storage capacity, and so on) as model inputs. The input-output model only works well for an undersaturated traffic environment because the queues often spread over the advanced detector.

Liu et al. (2009) proposed a real-time queue length estimation model considering five shockwave patterns: queuing shockwave, discharging shockwave, departure wave, compression shockwave, and new queuing shockwave with an uncleared cycle. The shockwave profile model (SPM) (Wu and Liu 2011) for congested arterial networks was developed by dividing traffic states into free-flow, saturated, and jammed conditions. The SPM assumes vehicles arrive at free-flow speed, discharge at the saturation flow rate, and the velocity for queue discharge shockwave is known. The two aforementioned shockwaves require high-resolution, accurate data input, which may comprise the models' performance due to data quality issues.

The stopbar and advanced detectors were combined to examine an arterial fundamental diagram (AFD) by Wu et al. (2011), described by a flow and occupancy diagram. With the information on detector distance and traffic signal timing, the occupancy time of the detector was used to identify breakpoints to estimate different traffic states. The paper implemented a microscopic car-following model (Newell 2002) to reconstruct vehicle trajectory from the stopbar detector. Their results showed that the flow-occupancy diagram can represent the traffic characteristics of the arterial link independent of the detector location. A simple method using only flow and occupancy at an advanced detector was developed for queue estimation. The model effect was evaluated in both simulated environment and field data. The results showed that the sensors closer to the intersection will yield better outcomes (Chang et al. 2013).

Cheng et al. (2011) used sampled trajectory data to estimate queue length by detecting critical points of state changes to convert the microscopic detections into macroscopic performance measurements. Queuing progression was formed by the arrival pattern; therefore, different arrival assumptions were made according to intersection control types. The method was evaluated against

simulated data set, next generation simulation (NGSIM) data set, and GPS data set. Sun and Ban (2013) applied mobile sensor data to reconstruct short vehicle trajectories around the intersection for the entire traffic flow at the signalized intersection. Their method is based on the variational formulation (VF) of kinematic waves developed by Daganzo (2005a, b) and solved using optimization-based and delay-based models.

Stopbar Detector and Performance Measures

Signal controller data only tell part of the story, and much of the information about intersection performance comes from the detection system. Stopbar video detectors recognize changes in the pixelation of a streaming image, thus allowing lane-by-lane detection without the need to install subsurface sensors. A system called TRANSFER was developed to determine the average queue length from detectors near the stopbar. A linear regression model was used to build the relationship between “fill-up” time with queue sizes, and the regression model was used to estimate upstream queue length (Mück 2002). Hallenbeck et al. (2008) analyzed the hypothesis that the stopbar detector combined with signal state data could be used to estimate arterial traffic conditions. They pointed out that using the stopbar detector was sufficient to evaluate intersection performance but not arterial performance. Although the delays were primarily intersection-based, the proposed method could approximate the arterial performance metric.

Rhodes et al. (2005) evaluated stopbar video detector accuracy by comparing the detector output from devices with high accuracy. Their results showed that stopbar video detectors tend to produce statistically significantly more false detections and miss detections. A more recent study (Moshiri and Montufar 2017) showed that three mainstream video detectors could perform well during ideal environmental conditions and are suitable for traffic data collection. The different evaluation results showed the improvement of video detection technologies in the last decade. As discussed by Emtinan and Day (2020), the configurations of detectors often vary in terms of the number of channels, detection zone length and distance, and approach- or lane-based detector assignment. Those authors examined those factors via a simulation model and provided practical recommendations for detector configurations.

Spatial Temporal Map

STMap Generation

The scanline method is a video analytic method in traffic-related research, which has been adopted broadly for traffic detection to

address the vehicle tracking problem of multicamera networks (Taniguchi et al. 1999; Dixon et al. 2009; Malinovskiy et al. 2009; Ardestani et al. 2016). More recent research applied the scanline method to extract high-resolution vehicle trajectories from high-angle traffic video to collect high-resolution trajectories (Zhang and Jin 2019). Studies also explored using the scanline and three-dimensional (3D) light detection and ranging (LiDAR) infrastructure for urban signalized intersections (Zhang et al. 2021b) and the 511 advanced traveler information system (Zhang et al. 2022).

The first step is defining the scanline on selected lanes and acquiring the pixel coordinates between each turning point. Next, the pixel value of the selected scanline will be accumulated, leading to the spatial-temporal map that shows the vehicle trajectories. The defined scanline and generated STMap are shown in Fig. 1.

STMap Coordinate Transformation

Due to the installation angle of the intersection CCTV camera, there is the perspective issue of raw STMap. As vehicles approached the intersection, the traveling trajectories in the farther location shown in STMap were distorted. In this step, we use perspective transformation to rectify STMap so that STMap can reflect the accurate traveling distance. We can obtain the homography transformation matrix by matching feature points between the video image and the Google map. Next, the original STMap is converted to a real-world STMap. In Fig. 2, the nonstopped vehicle trajectories from the original STMap are rectified as straight lines, in line with the intuition that the free flow speed should be constant. Finally, a scale factor is used to convert pixel distance on the undistorted STMap to physical distance. In the proposed model, the physical STMap will be used to collect the observed shockwave speeds in traffic flow.

The preceding subsections reviewed relevant studies regarding signal performance measures, shockwave theory, and stopbar detector. Compared with existing research, the paper's contributions are summarized as follows:

- A turning point (TP)-based trajectory algorithm is developed to reconstruct traffic arrivals at the advanced location for fully actuated or semiactuated adaptive controlled intersection, where only a stopbar detector is available.
- A dynamic queuing shockwave estimation model is built to update intersection queuing speed in real time with detector's occupancy that can be used as input for queue length estimation and signal optimization.
- New performance measures are proposed combining stopbar detection and signal phase and timing as a novel coordination diagram, which can be used for signal timing diagnosis and

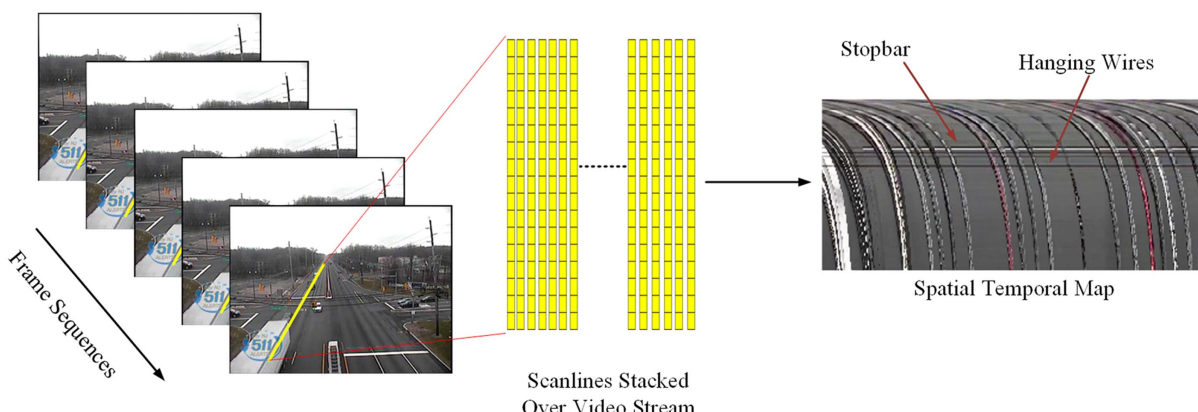


Fig. 1. Scanline and STMap generation (US1 at Henderson). (Images reprinted from NJDOT.)

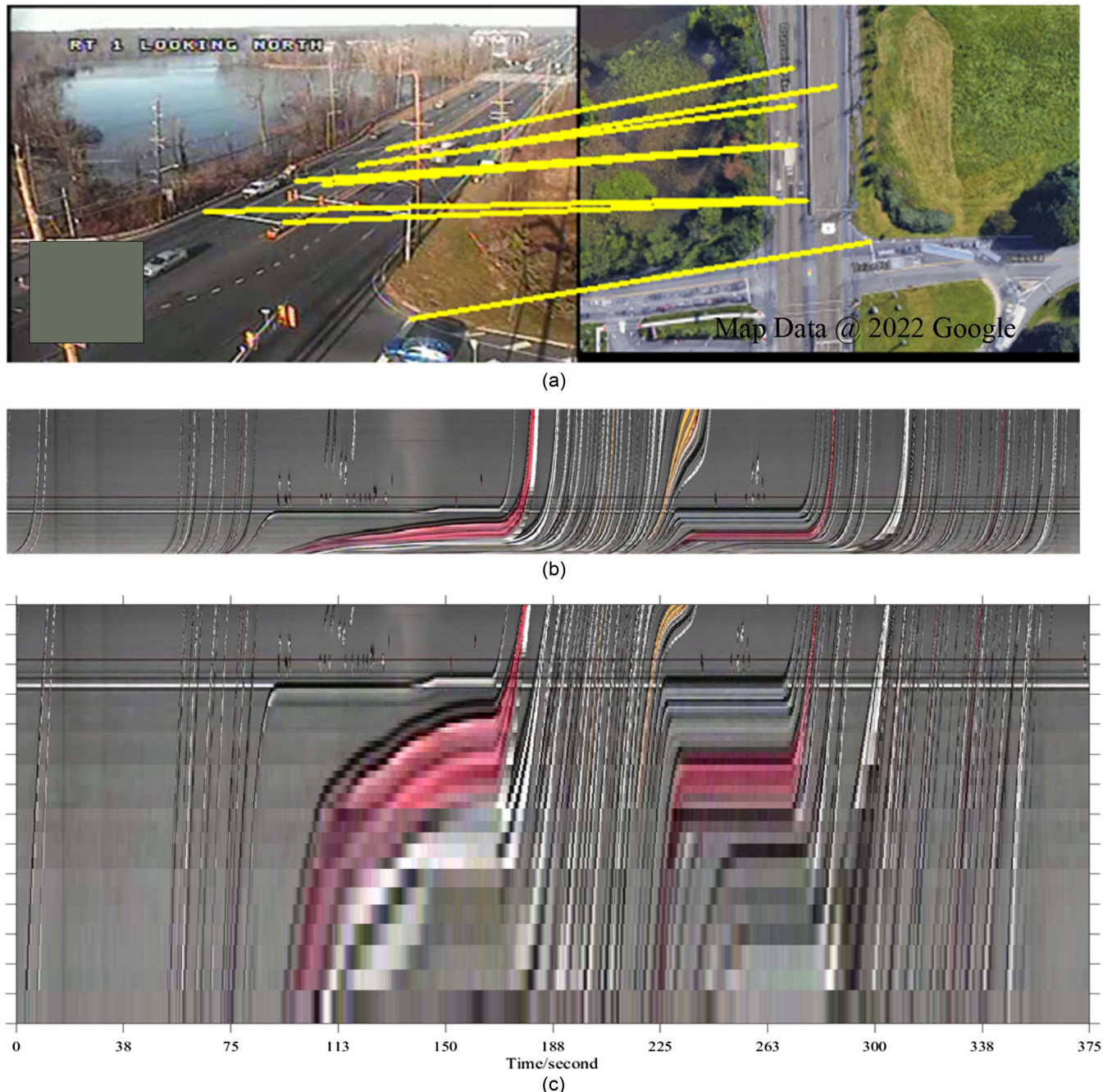


Fig. 2. Rectified STMap after perspective transformation using feature matching for US1 at Harrison: (a) feature matching between Google map and CCTV video (image reprinted from NJDOT; map data © 2022 Google); (b) original STMap; and (c) transformed STMap without perspective distortion.

overlaid with lane-by-lane vehicle trajectory data to show the traffic dynamics.

- Multiple data sources are explored, including CCTV roadside camera, Autoscope video detector, Wavetronix high-definition (HD) radar, and signal timing event log to integrate multiple data sources of traffic signal systems.

Methodology

In the “Methodology” section, the method to estimate state-changing points of vehicle trajectories is included. The reconstructed trajectory

data were then ingested into ATSPMs to produce targeted performance measures.

The shockwave speed is expressed as a ratio between the change of flow rate over the change of density, as shown in Eq. (1)

$$\omega = \frac{q_A - q_B}{k_A - k_B} = \frac{\Delta q}{\Delta k} \quad (1)$$

where q = flow rate; k = density; q_A and k_A = prior volume and density; and q_B and k_B = posterior volume and density.

Fig. 3 shows all types of shockwaves defining the boundaries of different traffic states. The following shockwave equations

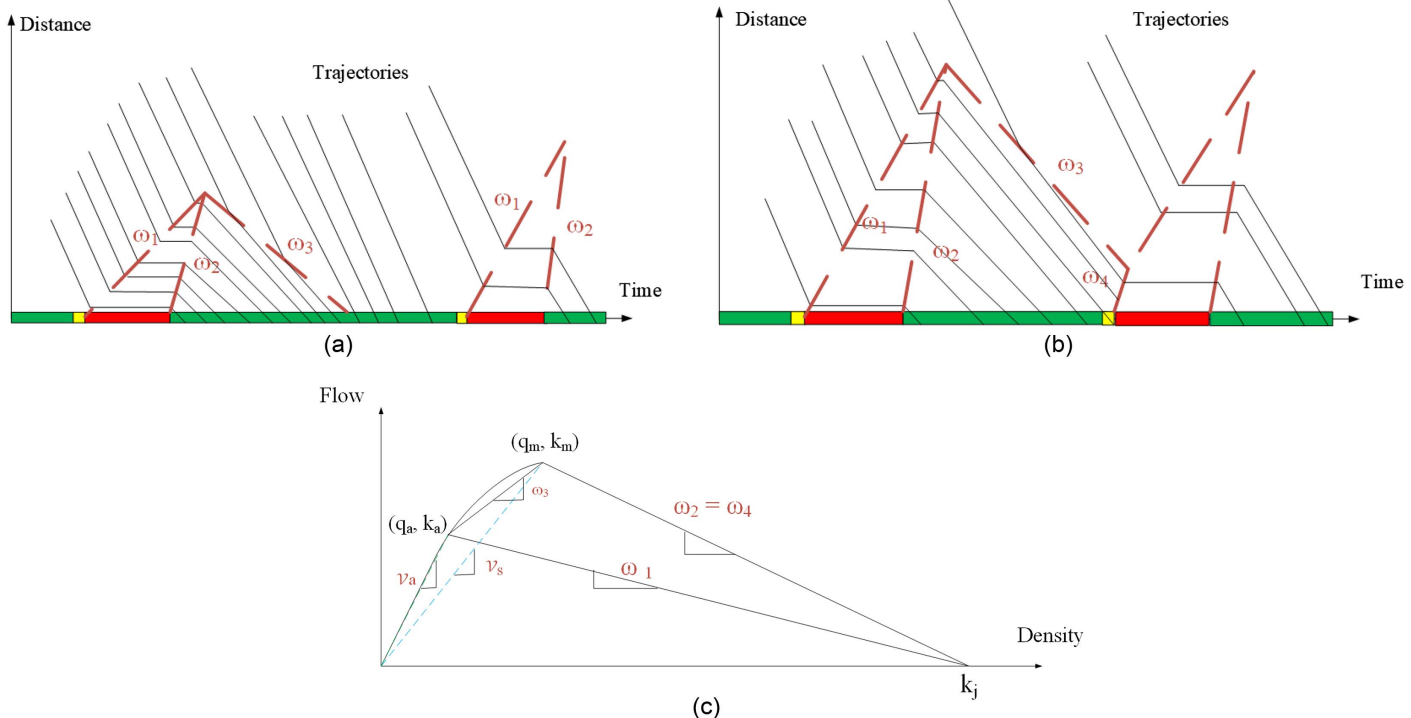


Fig. 3. Shockwave and fundamental diagram: (a) undersaturated conditions; (b) oversaturated conditions; and (c) fundamental diagram.

can be obtained based on Eq. (1). The equation for a queuing shockwave is

$$\omega_1 = \frac{q_a - 0}{k_a - k_j} \quad (2)$$

The equation for a discharging shockwave is

$$\omega_2 = \frac{0 - q_m}{k_j - k_m} \quad (3)$$

The equation for a propagating shockwave is

$$\omega_3 = \frac{q_a - q_m}{k_a - k_m} \quad (4)$$

The equation for a compression shockwave is

$$\omega_4 = \frac{q_m - 0}{k_m - k_j} \quad (5)$$

where q_a = arrival flow rate; q_m = maximum flow rate; k_m = maximum density at maximum flow rate; and k_j = jam density when vehicles are stopped. From the shockwave equations, we can find out that the discharging shockwave ω_2 , saturation flow speed v_s , and compression shockwave ω_4 are only impacted by the roadway design capacity and are independent of arrival flows.

The queuing shockwave is defined by the traffic state changing from arrival speed v_a to jam conditions. The discharging shockwave is defined by the traffic state changing from jam conditions to saturation flow. The propagating shockwave indicates that the arrival vehicles slow down from arrival speed to saturation flow. A compression shockwave is formed when queuing vehicles are not fully released during one cycle. The saturation flow rate is calculated by maximum flow divided by maximum density. In some literature (e.g., Sun and Ban 2013), the propagating shockwave ω_3 was considered the same as the free-flow speed. Other research

(e.g., Wu et al. 2011) treated ω_3 and free-flow speed differently. The discrepancy in calculating ω_3 from different papers depends on different shapes of fundamental diagrams used by the researchers.

This methodology of trajectory reconstruction contains two parts. The first part uses the scanline method to measure shockwave speeds. Then, the stopbar and signal phase and timing data are used to generate piecewise linear trajectories for vehicles passing through the intersection area.

Shockwave Speed Measurement Using STMap

Fig. 4 illustrates the STMap with converted physical distances. The shockwave patterns can then be observed for each signal cycle; ω_2 are stable because they are only related to lane characteristics, and ω_1 can be impacted by arrival flows, as shown in Eq. (2).

Because the queuing shockwave often varies from a different time of day and different cycle lengths, it is not sensible to use the same ω_1 all the time. To address the queuing shockwave speed (ω_1) estimation, a dynamic model was created to account for the fluctuation of traffic volume. The model can update queuing shockwave speed based on stopbar presence detection in real-time. The full derivation is as follows. From Eq. (2), we can get

$$\omega_1 = \frac{q - 0}{k - k_j} = \frac{q}{k} \times \left(\frac{1}{1 - \frac{k_j}{k}} \right) \quad (6)$$

given the speed-flow-density relationship

$$q = \mu \times k \quad (7)$$

By substituting the Eq. (7) into Eq. (6), we will obtain the following relationship:

$$\omega_1 = \mu \times \left(\frac{1}{1 - \frac{k_j}{k}} \right) \quad (8)$$

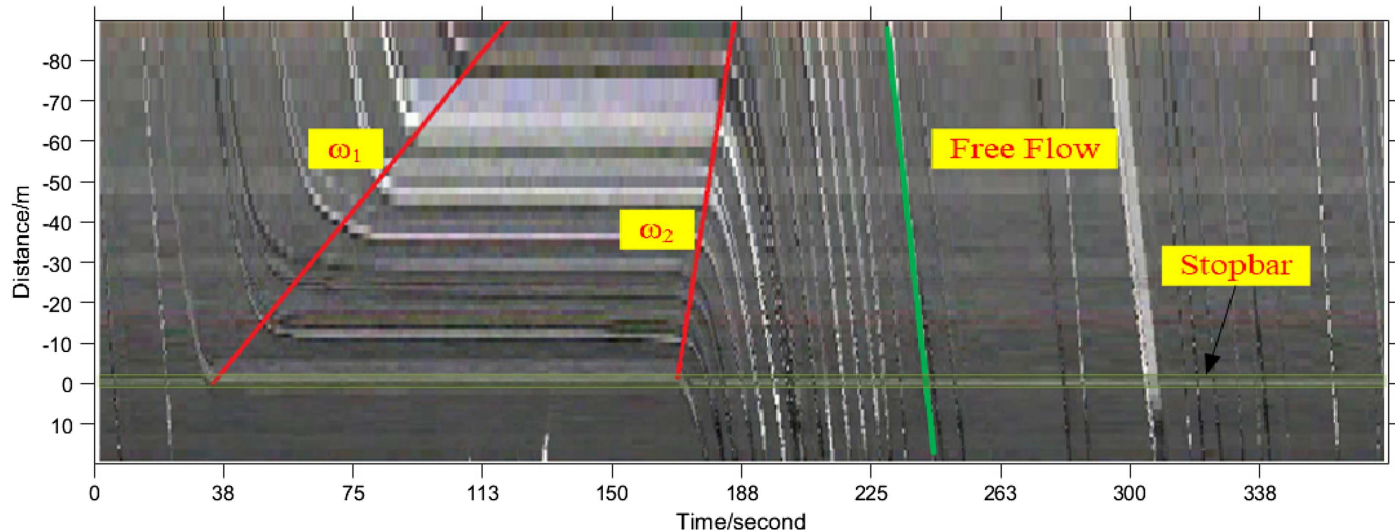


Fig. 4. Shockwave measurements from STMap. ω_1 = queuing shockwave and ω_2 = discharging shockwave. (Images by Tianya Zhang.)

Assuming the fundamental diagram is given by the speed-density relationship

$$\mu = \mu(k) \quad (9)$$

it follows that

$$\omega_1 = \mu(k) \times \left(\frac{1}{1 - \frac{k_j}{k}} \right) \quad (10)$$

As discussed in many previous studies (Hall and Persaud 1989; Hall 1996; Cassidy 1998), occupancy and density are almost constant multiples of each other, assuming consistent average vehicle length. That is, from the stopbar detectors' occupancy measure, Occ , for each lane, we can obtain Eqs. (11)–(13)

$$k = g \times \text{Occ} \quad (11)$$

$$\frac{\text{Occ}}{\text{Occ}_o} = \frac{k}{k_o} \quad (12)$$

$$\frac{\text{Occ}_j}{\text{Occ}} = \frac{k_j}{k} \quad (13)$$

where g = factor that converts occupancy into density; Occ_o = optimal stopbar occupancy corresponding to maximum flow density; and Occ_j = jam occupancy.

Then, ω_1 can be further written

$$\omega_1 = \mu(g \times \text{Occ}) \left(\frac{1}{1 - \frac{\text{Occ}_j}{\text{Occ}}} \right) \quad (14)$$

In this way, we establish a relationship between shockwave speed ω_1 with the occupancy observed at the stopbar detectors. By applying different speed-density relationships $u = \mu(k)$, we can then estimate the dynamic speed of the ω_1 shockwave in response to different queue spacing conditions, which can vary significantly in arterial streets.

We conducted some preliminary analysis of several different speed-density relationships (Fig. 5). Based on the model evaluation results with observed field data, the Underwood exponential model captured the trend better among all candidate models, including

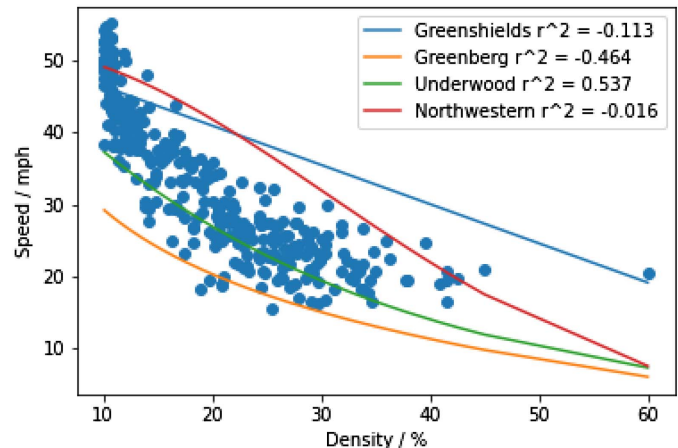


Fig. 5. Comparison of different speed-density models with field data.

Greenshields linear, Greenberg logarithmic, and Northwestern models (Greenshields et al. 1935; Underwood 1961; Greenberg 1959).

The Underwood model is expressed

$$\mu = \mu_f \times e^{-\frac{k}{k_o}} \quad (15)$$

where μ_f = free-flow speed; and k_o = optimum density corresponding to the maximum flow. Given Eq. (12), we can substitute the ratio of density in Eq. (14) with Eq. (15). The following equation holds:

$$\omega_1 = \mu_f \times e^{-\frac{\text{Occ}}{\text{Occ}_o}} \times \left(\frac{1}{1 - \frac{\text{Occ}_j}{\text{Occ}}} \right) \quad (16)$$

where ω_1 = real-time queuing shockwave to be determined; μ_f = free-flow speed; Occ = stopbar occupancy during the green phase; Occ_o = occupancy under optimum flow; and Occ_j = occupancy under jam traffic.

The preceding derivation showed that we can estimate the queue forming speed with single detectors' occupancy for signalized intersections. QED.

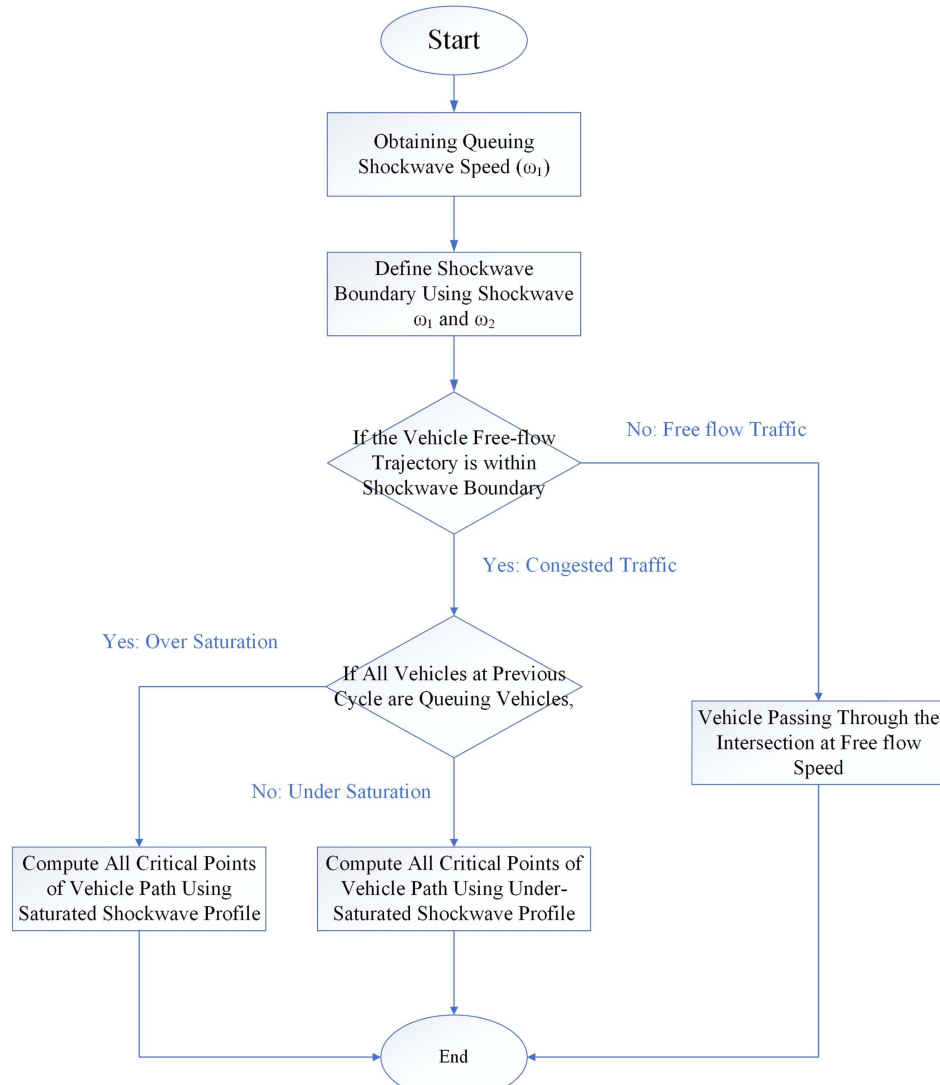


Fig. 6. Workflow for trajectory reconstruction based on shockwave profile.

Stopbar Trajectory Reconstruction

The turning point-based trajectory estimation algorithm contains two branches, where one is for undersaturated conditions, and the other is for the oversaturated condition (Fig. 6).

Determine Shockwave Triangular Boundary

The key to reconstructing the vehicle trajectories is identifying all turning points of the piecewise linear trajectory model. After obtaining ω_1 and ω_2 , the queuing distance and shockwave boundary can be calculated, which are used to determine whether a vehicle is stopped or passing through at free-flow speed. The intersecting point of two shockwaves is calculated as follows:

$$t_{\text{boundary}} = \frac{\omega_2 \times t_{\text{depart}}^1 - \omega_1 \times t_{\text{arrival}}^1}{\omega_2 - \omega_1} \quad (17)$$

$$d_{\text{boundary}} = (t_{\text{arrival}}^1 - t_{\text{queue}}) \times \omega_1 \quad (18)$$

where t_{boundary} and d_{boundary} = timestamp and location of converging point between ω_1 and ω_2 ; ω_1 and ω_2 = queuing and discharging shockwaves; t_{arrival}^1 = first vehicle arrival timestamp; and t_{depart}^1 = first vehicle departing timestamp.

Determine Turning Points of Queuing Vehicles for Undersaturated Conditions

Fig. 7 shows the turning points of vehicle trajectories and shockwave triangle for undersaturated conditions. TP0 is when a vehicle

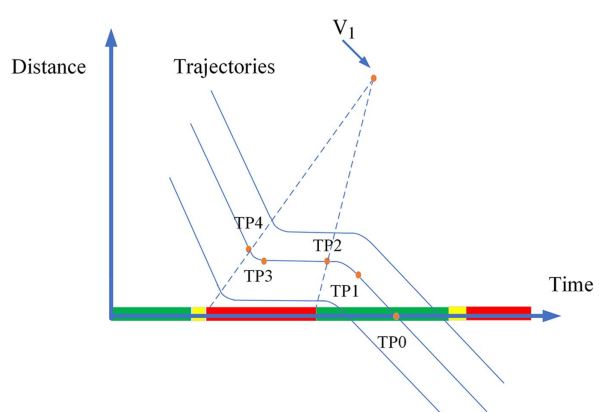


Fig. 7. Undersaturated conditions: turning points used for trajectory reconstruction.

passed through the stopbar; TP1 is when the car accelerated to the saturation flow speed; TP2 is when the vehicle starts to move; TP3 is when the car stopped; TP4 is when the car begins to decelerate; and $V1(t_{V_1}, d_{V_1})$ is the converging point between queuing and discharging shockwaves.

The first step is to calculate each queuing vehicle's joining and departing point when the queuing and discharging shockwaves propagate to the queued vehicle. This is a simplified macroscopic level model, which accounts for the inherent linear property of shockwaves.

First, TP0 is computed, the timestamp of a vehicle passing the intersection

$$t_{TP0}^i = t_{stopbar}^i \quad (19)$$

$$d_{TP0}^i = 0 \quad (20)$$

Second, TP2 is computed when the vehicle starts to accelerate until its speed reaches the free-flow speed

$$t_{TP2}^i = \frac{\frac{v_s^2}{acc} - v_s \times t_{stopbar}^i + w_2 \times t_{green}^{begin} - \frac{1}{2} \times acc \times \left(\frac{v_s}{acc}\right)^2}{\omega_2 - v_s} \quad (21)$$

$$d_{TP2}^i = w_2 \times (t_{TP2}^i - t_{green}^{begin}) \quad (22)$$

Upon obtaining TP2, TP1 is calculated once the vehicle reaches the saturation flow speed

$$t_{TP1}^i = t_{TP2}^i + \frac{v_s}{acc} \quad (23)$$

$$d_{TP1}^i = v_s \times (t_{TP1}^i - t_{stopbar}^i) \quad (24)$$

TP3 is determined when the queuing vehicle stops and joins the queue. To calculate TP3, the nonhomogeneous Poisson is used to capture the randomness of arrival patterns because vehicle arrival rates vary during different times of the day. Under certain heavy vehicle conditions, however, the normal distribution arrival model captures the high-volume vehicle arrival patterns. For a nonhomogeneous Poisson process with rate $\lambda(t)$, the number of arrivals in any interval, at any point along the corridor, is a time-dependent random variable. The homogeneous or nonhomogeneous Poisson distribution for modeling vehicle arrivals has been used as the commonly seen choice in many published studies (Osorio and Wang 2017; Wang et al. 2017). The number of vehicle arrivals between time interval s is expressed

$$N(t+s) - N(t) \sim \text{Poisson} \left(\int_t^{t+s} \lambda(\alpha) d\alpha \right) \quad (25)$$

The arrival headway Δ_i between consecutive two vehicles is defined

$$\Delta_i = t_2 - t_1, \text{ subject to } N(t_2) - N(t_1) = 1 \quad (26)$$

where $N(t), t \in [0, \infty]$ = counted number of vehicles arrivals. For a Poisson process, it has to suffice two conditions, namely the time intervals between Poisson events that occur at the rate of λ per unit of time are (1) mutually independent, and (2) described by an exponential distribution function with parameter λ . Given the segment between the testing location at Route 1 and Harrison and upstream Route 1 and Independence has a distance of over 3 km (2 mi). It is reasonable to consider the arrival of the vehicle is an uncoordinated process. For platoon vehicles, the normal distribution is more suitable.

Therefore, TP3 is obtained with the following equations:

$$t_{TP3}^i = t_{arrival}^1 + \sum_{k=2}^{i-1} \Delta_k \quad (27)$$

$$d_{TP3}^i = d_{TP2}^i \quad (28)$$

TP4 is when the vehicle starts to decelerate, which is considered the arrival of the red event

$$t_{TP4}^i = t_{TP3}^i - v_f / dec \quad (29)$$

$$d_{TP4}^i = d_{TP3}^i - 0.5 \times dec \times \left(\frac{v_f}{dec}\right)^2 \quad (30)$$

where w_1 = queuing shockwave speed; w_2 = discharging shockwave; v_f = free-flow speed; v_s = saturation flow speed; acc = acceleration rate [m/s^2 (ft/s^2)]; dec = deceleration rate (ft/s^2); $t_{stopbar}^i$ = timestamp of the i th vehicle passing the stopbar detector; and t_{green}^{begin} = green phase begin time.

Finally, all critical points are connected to reconstruct the piecewise linear vehicle trajectories. By obtaining vehicle trajectories from stopbar detector data, the vehicle arrival timestamps can be obtained as input for signal performance measurements such as PCDs even though there is no available advanced detector at the intersection.

Determine Turning Points of Queuing Vehicles for Saturated Conditions

Fig. 8 shows the turning points of vehicle trajectories and shockwave triangles at oversaturated conditions, meaning the queuing vehicles cannot be released from the previous green phase. TP0, TP1, TP2, and TP3 are the same as for undersaturated conditions. TP4 is when the vehicle begins to decelerate on a compression shockwave; TP5 is when a vehicle reaches the saturation flow speed at the previous cycle; TP6 is when the car starts to move in the previous cycle; TP7 is when the vehicle completely stopped in the previous cycle; TP8 is when the car begins to slow down in the previous cycle. $V1(t_{V_1}, d_{V_1})$ is the converging point between queuing and discharging shockwaves. $V2(t_{V_2}, d_{V_2})$ is the converging point between compression and queuing shockwaves.

If the previous cycle is oversaturated and the vehicle at free-flow speed will avoid the shockwave boundary, this vehicle is considered to pass the intersection at free-flow speed. Otherwise, the following equations can be used to calculate TP4, TP5, TP7, and TP8.

If the previous cycle is oversaturated, and the calculated TP2 and V2 meet the condition $|d_{TP2}^i| \leq |d_{V_2}|$, which means this vehicle joined the compression shockwave during the current cycle, then the following equations Eqs. (31) and (32) are used to calculate TP4. If the vehicle does not join the compression shockwave, TP4 is calculated using Eqs. (29) and (30)

$$t_{TP4}^i = t_{TP3}^i - v_s / dec \quad (31)$$

$$d_{TP4}^i = d_{TP3}^i - 0.5 \times dec \times \left(\frac{\mu_s}{dec}\right)^2 \quad (32)$$

TP6 is computed when the vehicle starts to accelerate using the previous cycle's parameters

$$t_{TP6}^i = \frac{\frac{v_s^2}{acc} - v_s \times t_{TP4}^i + w_2 \times t_{green}^{previous begin} - \frac{1}{2} \times acc \times \left(\frac{v_s}{acc}\right)^2}{\omega_2 - v_s} \quad (33)$$

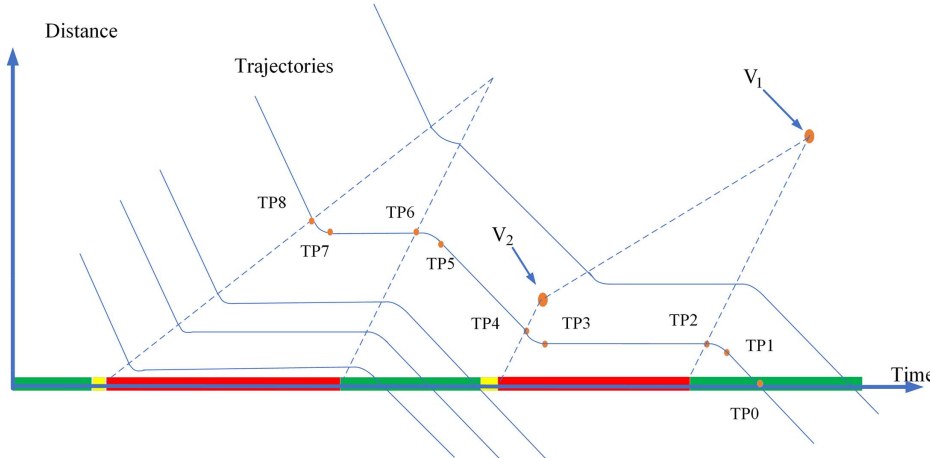


Fig. 8. Saturated conditions: turning points used for trajectory reconstruction.

$$d_{TP6}^i = w_2 \times (t_{TP6}^i - t_{\text{green}}^{\text{previous begin}}) \quad (34)$$

TP5 is when the vehicle reaches the saturation flow speed, which can be obtained using the next equations

$$t_{TP5}^i = t_{TP6}^i + \frac{v_s}{\text{acc}} \quad (35)$$

$$d_{TP5}^i = v_s \times (t_{TP5}^i - t_{TP4}^i) \quad (36)$$

Therefore, TP7 is obtained with the following equations based on the Poisson arrival pattern and the first arrival vehicle's timestamp at the previous cycle. In an oversaturated condition, the current cycle's i th queuing vehicle is the j th queuing vehicle in the previous cycle

$$t_{TP7}^i = t_{\text{arrival}}^{\text{previous}-1} + \sum_{k=2}^{k=\text{previous}-j} \Delta_k \quad (37)$$

$$d_{TP7}^i = d_{TP6}^i \quad (38)$$

TP8 is the vehicle starting to decelerate at the previous cycle

$$t_{TP8}^i = t_{TP7}^i - v_f/\text{dec} \quad (39)$$

$$d_{TP8}^i = d_{TP7}^i - 0.5 \times \text{dec} \times \left(\frac{v_f}{\text{dec}} \right)^2 \quad (40)$$

where $t_{\text{green}}^{\text{previous begin}} = \text{green begin timestamp in the previous cycle}$; and $t_{\text{arrival}}^{\text{previous}-1} = \text{first vehicle arrival timestamp in previous cycle}$.

Spatial-Temporal Map with Stopbar Detector Data

We designed a trajectory comparison method to visually evaluate the reconstructed trajectory by plotting the estimated vehicle trajectory on STMap. This innovative way of vehicle trajectory visualization significantly reduces the complexity of validating vehicle detection results. As shown in Fig. 9, the pixel strands are physical vehicle trajectories captured on STMap, which are used as ground-truth vehicle trajectories to evaluate the model results. The stopbar detector on/off is also plotted on the STMap to show the duration of the vehicle passing by the Autoscope stopbar detection zone. The STMap can capture accurate spatial and temporal information and will become an important tool for traffic measurements.

Experiment Implementation

In the first phase of the project (Jin et al. 2019), the ATSPMs were successfully built on existing adaptive systems from the

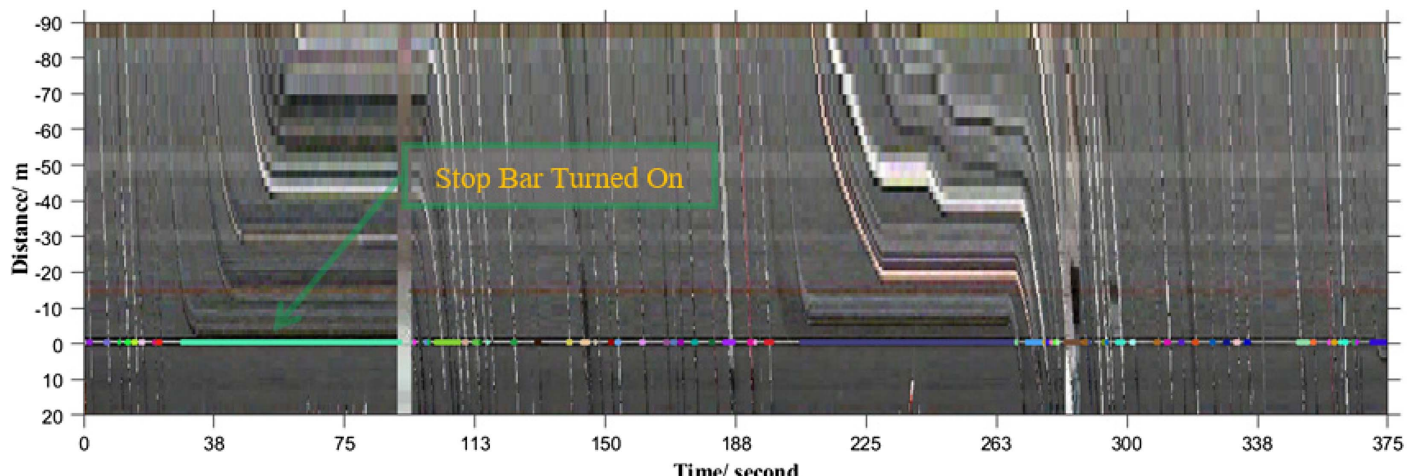


Fig. 9. CCTV STMap trajectory with stopbar on/off.

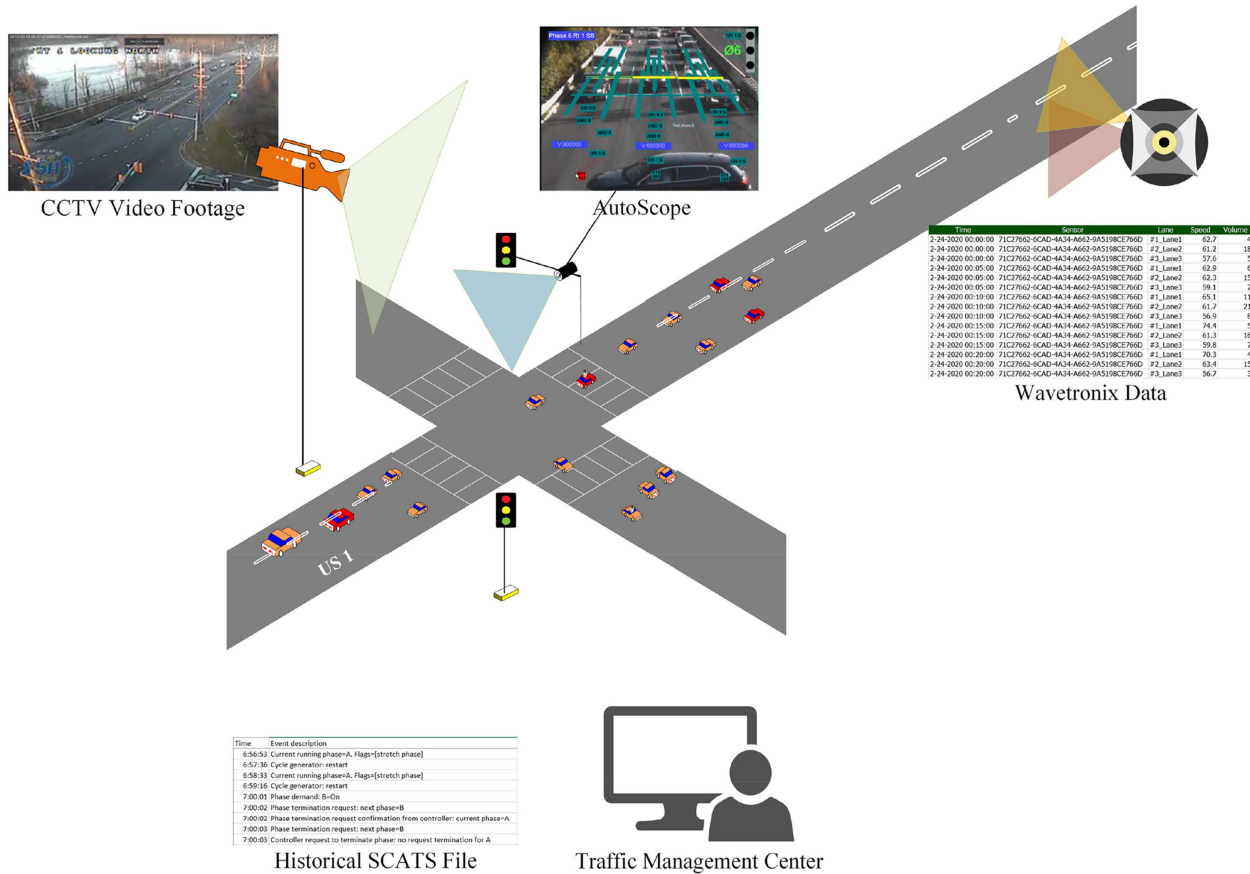


Fig. 10. Multisource data collected for intersection performance measurement. (Images reprinted from NJDOT.)

centralized management console instead of configuring at each controlled intersection on the field. The developed framework has been designed, implemented, and tested for two adaptive signal systems, SCATS and InSync on two selected corridors in New Jersey. The proposed method utilizes existing detection system to ingest into ATSPMs without investment in new controllers and detectors. Thus, the solution can help agencies focus on functionality in a legacy system instead of needed detectors/controller types.

Data Collection

The SCATS system featured two layers of control logic: strategic level and tactical level. The local controller was used to determine a single intersection phase and time, and the regional controller was used to adjust coordination between junctions. The SCATS can be used for data collection, control, and traffic modeling through its intelligent transportation system (ITS) interface with third-party applications. The collected data contains the signal controller event history file, Autoscope detector data, and roadside CCTV camera video, which can be accessed through the traffic management center. An upstream Wavetronix HD radar detector (Wavetronix LLC, Springville, Utah) were also used to obtain corridor level traffic flow parameters. The data sources are shown in Fig. 10.

Signal Event History File

The data are from a SCATS-controlled intersection on US-1 at Harrison in New Jersey. In addition, 2 days of SCATS event data and Autoscope detector data were recorded, which spanned from December 2 to December 4, 2020.

Autoscope Detector Data

The Autoscope Vision detection system contains a high-definition camera-processor sensor that delivers reliable counting results for stopbar vehicle detection. The Autoscope stopbar video detectors were recorded from the arterial traffic management center. The Autoscope detector data file contains detector id for each lane, timestamps of detector state change, and metadata regarding the detector settings.

CCTV Camera Recordings

The 511 CCTV camera network is a critical ITS infrastructure for the advanced traveler information system. The CCTV video from the NJ511 camera network and CCTV data were recorded into several 1-h clips to record real traffic situations. In addition, the CCTV video data were used to get initial measurements for shockwaves, free-flow speed, and other physical parameters.

Wavetronix HD Radar Data

The Wavetronix HD radar detection system was installed in proximity (1,200 ft) that monitors traffic flow conditions, providing lane-by-lane detection results at 5-min intervals but not for signal timing purpose. Three microscope traffic flow parameters were reported, including speed, volume, and occupancy. It also reported vehicle types, headway, and distance gaps at the microscopic level. From Wavetronix data, we can measure the optimal occupancy (Occ_o) and maximum occupancy (occ_j). The flow-occupancy and speed-volume data are plotted in Fig. 11.

With all the data from different sources, a preprocessing step was conducted to convert data into the standard format. For example, the SCATS history log files, which preserve the signal phase

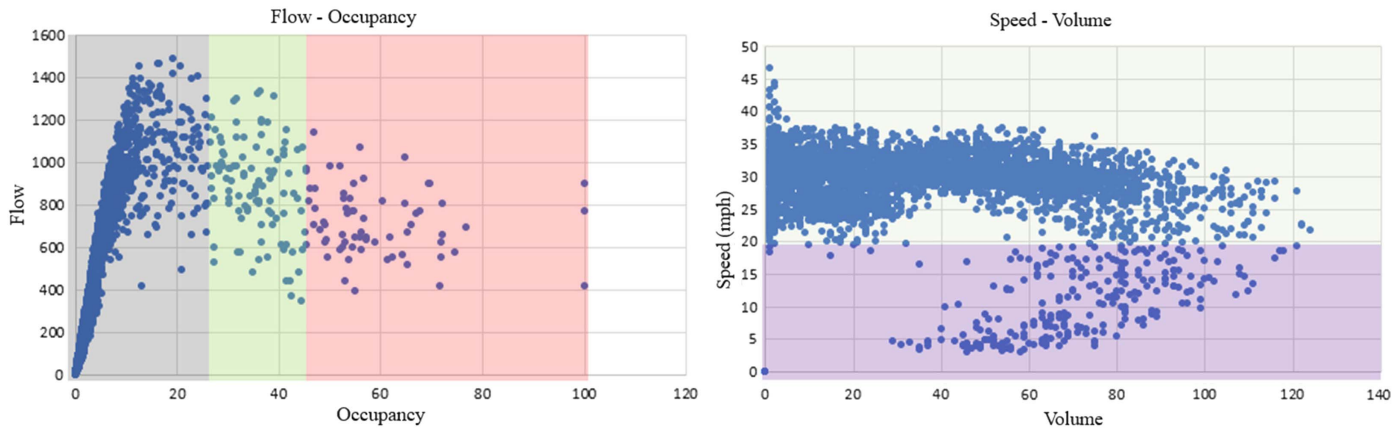


Fig. 11. Flow-occupancy and speed-volume plot from Wavetronix data.

and timing information, were firstly converted into standard ATSPMs event code through an event translator program (Jin et al. 2019). After the data collection and transformation, the detection and signal events are then ready to generate performance measurements with the aforementioned algorithms. Because the advanced detection system in this setting is not used for signal performance purposes, we recover the vehicle arrivals at the advanced detector location through the proposed trajectory estimation method.

Model Analysis

In this section, we present the results of reconstructed vehicle trajectories and a combination of stopbar detector, signal phase, and timing (SPaT) to generate performance measures.

Parameter Optimization

As shown in Fig. 12(a), a lateral scanline was placed in the video as an advanced detector to collect the actual vehicle arrivals from CCTV video footage. The timestamp of each passing vehicle was extracted after marking the passing cars from the lateral scanline. Fig. 12(b) illustrates the semiautomated tool developed to automatically extract the manually marked timestamp of each passing vehicle from the lateral scanline. The collected vehicle arrivals were used as ground-truth data to calibrate and evaluate our model performance.

Traffic parameters used in the model include three shockwave speeds, free-flow speed, acceleration rate, deceleration rate, and average vehicle arrival headway. Each parameter was first measured from a spatial-temporal map. Then, the measured values of traffic flow parameters were optimized using the genetic algorithm. The goal function of the genetic algorithm is defined as follows:

$$f(X) = \frac{\text{True Positives}}{\text{True Positives} + \text{False Positives}} \quad (41)$$

$$Z = \text{argmax}(f(X)) \quad (42)$$

The genetic algorithm is used to obtain the optimal parameter set Z by maximizing function $f(X)$

$$\text{True Positives}(\tau_d) = \begin{cases} 1, & \text{if } \forall \bar{\tau}_d \mid \tau_d - \bar{\tau}_d \mid \leq \varepsilon_r \\ 0, & \text{otherwise} \end{cases} \quad (43)$$

$$\text{False Positives}(\tau_d) = \begin{cases} 1, & \text{if } \forall \bar{\tau}_d \mid \tau_d - \bar{\tau}_d \mid \geq \varepsilon_r \\ 0, & \text{otherwise} \end{cases} \quad (44)$$

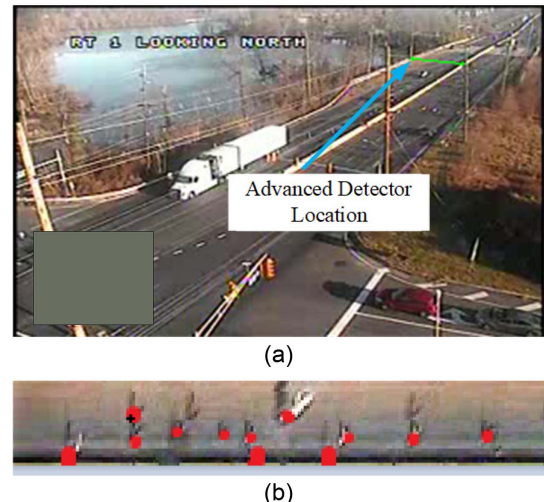


Fig. 12. Virtual line detection to collect vehicle arrivals at advanced detector: (a) lateral scanline as advanced detector; and (b) manually marked passing vehicles. (Images reprinted from NJDOT.)

where ε_r = error threshold. The τ_d = timestamp of reconstructed trajectory at the advanced detector; and $\bar{\tau}_d$ = ground-truth timestamp when a vehicle is passing through the advanced detector from CCTV video.

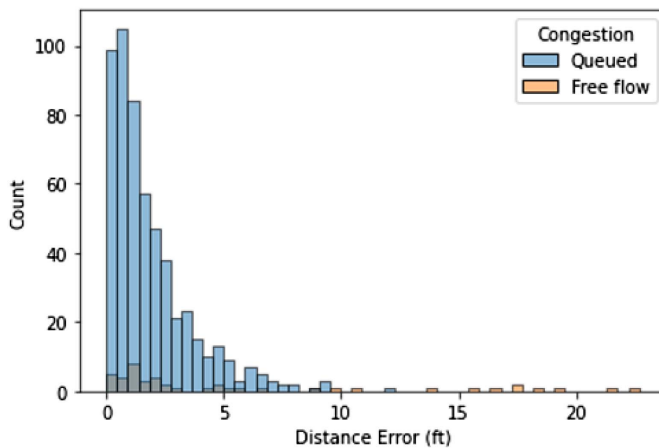
The initial parameter values and calibrated parameter values are presented in Table 1.

To evaluate advanced detector data using reconstructed vehicle trajectories from stopbar detector data, we calculated the distance error for model output trajectory with video recorded trajectory at the advanced detector in Fig. 13. Our algorithm has very good accuracy that the majority of detected trajectories had distance error ≤ 5 ft compared with ground-truth vehicle trajectory. The primary error source comes from the Autoscope video detector. According to our manual validation results using the raw Autoscope video, about 5%–10% of vehicle detection errors existed in the stopbar detection system.

To illustrate how the detector errors would impact our model performance, we compared the model outputs results using CCTV-video-collected stopbar events and Autoscope stopbar detector events, respectively. Fig. 14 presents the positive detection rates for different error thresholds. The figure of positive detection rates shows that manually counting vehicle stopbar events had a lower

Table 1. Parameter optimization using genetic algorithm

| Model parameters | Initial value | Calibrated value |
|--|---------------|------------------|
| Discharging shockwave, w_2 (ft/s) | -25.54 | -22.29 |
| Optimal occupancy, Occ^o (%) | 30.5 | 24.1 |
| Maximum occupancy, Occ^J (%) | 95 | 90.4 |
| Saturation flow rate, v_s (ft/s) | 29.40 | 32.08 |
| Free-flow speed, v_f (ft/s) | 51.93 | 44.92 |
| Acceleration rate (ft/s ²) | 13.12 | 12.39 |
| Deceleration rate (ft/s ²) | 26.25 | 24.19 |
| Mean arrival headway (s) | 4.0 | 3.0 |

**Fig. 13.** Trajectory algorithm distance error for congested vehicles and free-flow vehicles.

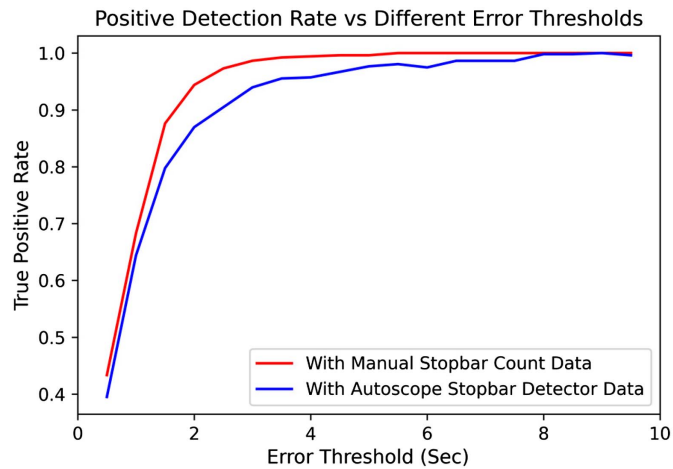
trajectory detection error. The proposed model can accurately reconstruct about 90% of advanced detections with a 2-s discrepancy between ground-truth and reconstructed data. The model outputs can achieve about 95% at a 4-s error threshold. Because the legacy Autoscope video detector still uses traditional motion detection, it inevitably results in many false detection and missed detection issues. However, with the adoption of advanced computer vision algorithms, this error source is expected to be significantly reduced in the new video detection system.

To demonstrate the accuracy of model results by visualization, the reconstructed vehicle trajectories, stopbar detector events, and advanced detector position are plotted on the STMap (Fig. 15). For example, in the same figure, each dot on the stopbar represents the detection of one vehicle passing through the stopbar detection zone. A line is placed at the advanced detector location, 400 ft away from the intersection. The trajectory diagram shows how well our estimated trajectories align with the actual vehicle movements in the STMap. The detailed TP-based vehicle trajectory plotting algorithm is in the Appendix.

Because this method tries to reconstruct vehicle trajectories from a macroscopic perspective, the randomness of driver behavior was not considered. For instance, the lane-changing event will be missed using this method. Future work will combine the GPS-connected vehicle trajectory data with stopbar detector data to solve the randomness in vehicle trajectory.

Purdue Coordination Diagram from Reconstructed Trajectory

After obtaining all trajectories, vehicle arrivals at the upstream location can be estimated for the advanced detection-based

**Fig. 14.** True positive rate over different error thresholds.

performance measurements (Fig. 16). The first PCD diagram shows the collected vehicle arrivals from CCTV video. The second PCD diagram is predicted detector data from the reconstructed trajectory. The high percentage of vehicle arrivals on green time implies fewer vehicle stops. By comparing the two diagrams, it shows that the trajectory reconstruction method has the same arrival on green (AoG) value as the vehicle arrivals recorded from CCTV camera, indicating that the proposed method can efficiently recover upstream vehicle movements from the stopbar detector actuation. Solid dots are darker in the PCD with ground-truth vehicle arrivals than algorithm generated vehicle arrivals. The stopbar detector tends to undercount, resulting in less vehicle counting due to occlusions in the Autoscope camera.

In Fig. 17, 24-h PCDs from four intersections were created using the stopbar-based estimation algorithm. The PCD diagrams show that our proposed method can be efficiently deployed at large scale from the centralized management console.

Rutgers Coordination Diagram

The detector data tell the system when the vehicles arrive and leave the intersection, which is an essential part of traffic monitoring systems. Combined with high-resolution phase and timing data, the stopbar detector data provide insights into how the signal controller functions to accommodate various traffic demands. The stopbar coordination diagram was created as a new signal performance measurement containing important information, such as vehicle departure headways, waiting time, delay, phase duration, volume, and occupancy. Because the advanced detections for signalized intersections are primarily deployed on the main street with high-speed approaches [65 km/h (40 mi/h) or higher] for dilemma zone analysis, agencies using the same advanced detection for PCDs reap additional benefits. Compared with the PCD, the stopbar detector can benefit the side-street and arterial low-speed approaches that often do not have advanced detectors.

Different from the timing and actuation diagram that included an advanced detector, stopbar detector, and pedestrian button actuation time, by focusing only on stopbar detection, the Rutgers coordination diagram (RCD) tries to emphasize the detector occupancy parameter (Fig. 18). From the new coordination diagram, the effectiveness of the signal timing can be quickly diagnosed using the time headways. A significant time gap usually implies that the queuing vehicles were cleared. Therefore, vehicles arriving on green do not need to stop during that cycle. However, if all gaps

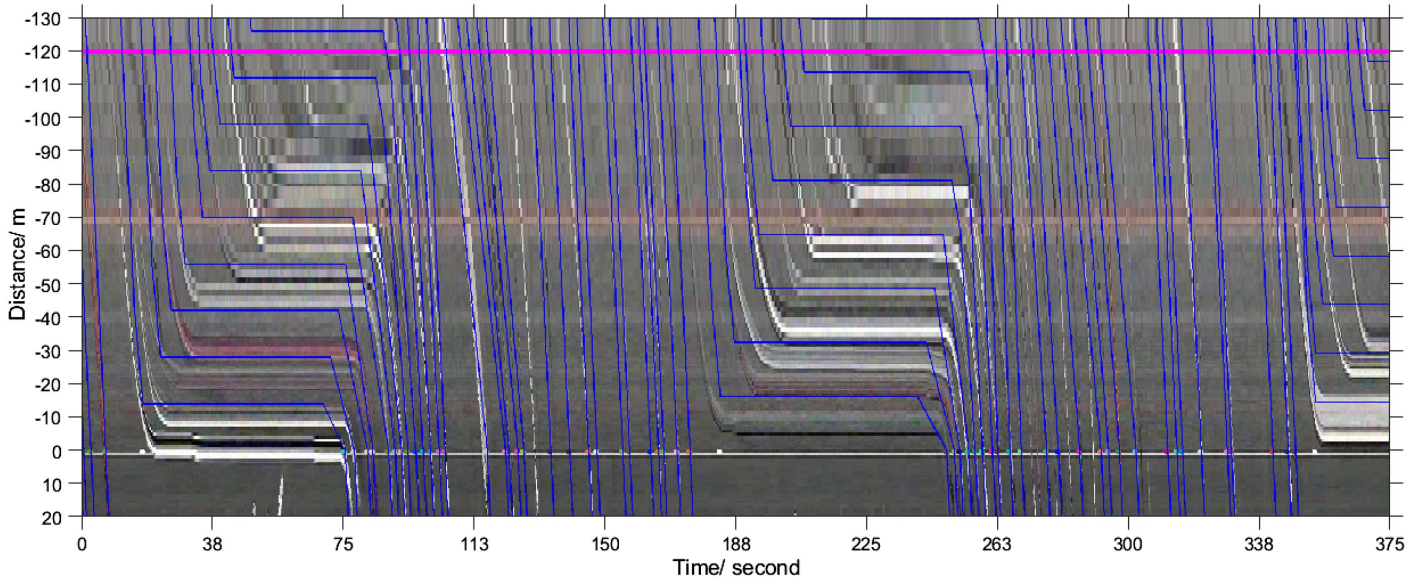


Fig. 15. Reconstructed trajectory and stopbar detector plotted on STMap.

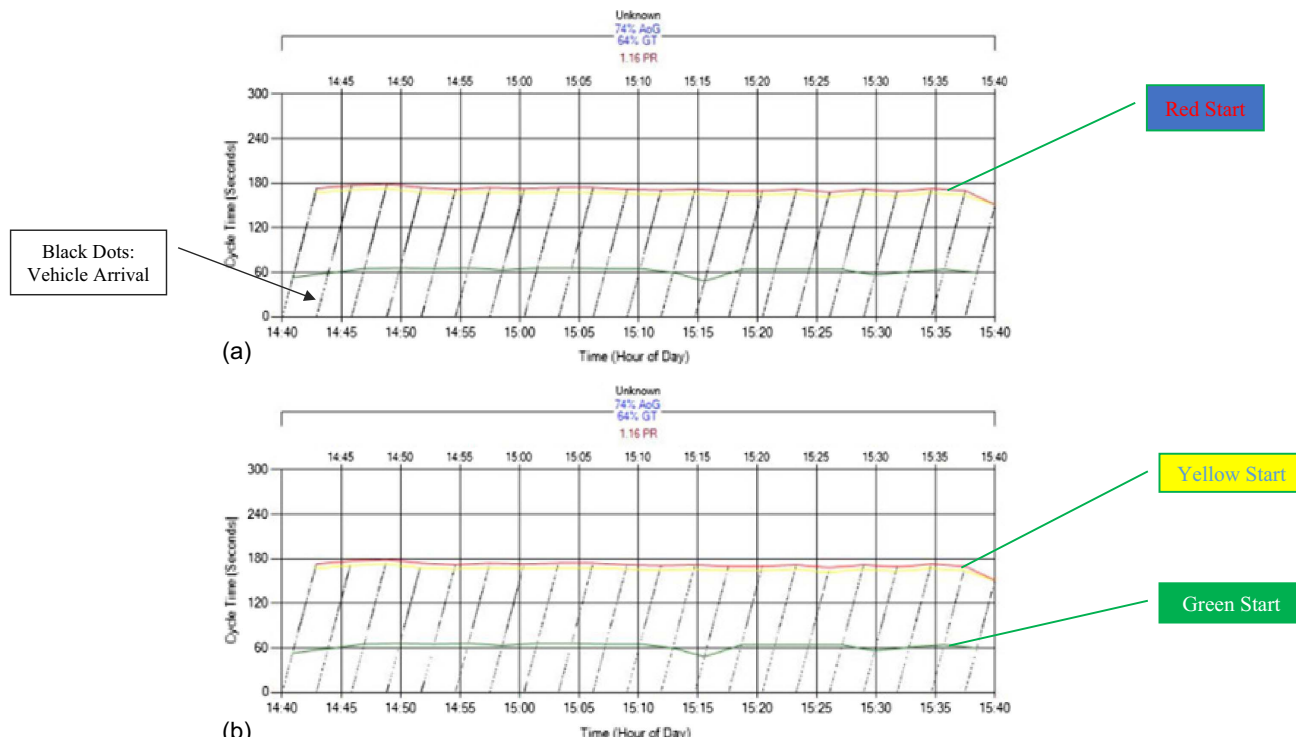


Fig. 16. Purdue coordination diagram using reconstructed trajectory: (a) PCD with ground-truth advanced detection; and (b) PCD with algorithm advanced detection.

within one cycle are very small and almost constant, a split failure was considered as the queuing vehicles are unable to be cleared.

Split failure can be identified using a combination of green occupancy ratio (GOR) and red occupancy ratio for the first 5 s of red (ROR5) (Day et al. 2014). Green occupancy is the percentage of green time for which the stopbar sensor was switched on. Red occupancy is defined as the ratio of the first 5 s of red time for which the stopbar sensor was turned on. A high GOR along with a high ROR5 value means that the queue from the last cycle was not cleared, resulting in a split failure. Another way to detect the end

of the queue using a stopbar detector is to find the large gap, which is greater than the site-specific threshold depending on road geometry and traffic composition. In many practices, the time to gap out (TTG) as the queue end indicator is set as 2 s (Smaglik et al. 2017). Considering vehicle trajectory data from connected vehicles or our turning point-based trajectory reconstruction algorithm, the RCD can be effortlessly converted to a time-space diagram, where the high-resolution trajectories can be placed to show the progression of traffic flow. The plotted lane-by-lane trajectory shows one cycle duration from Phase 6 (Fig. 18).

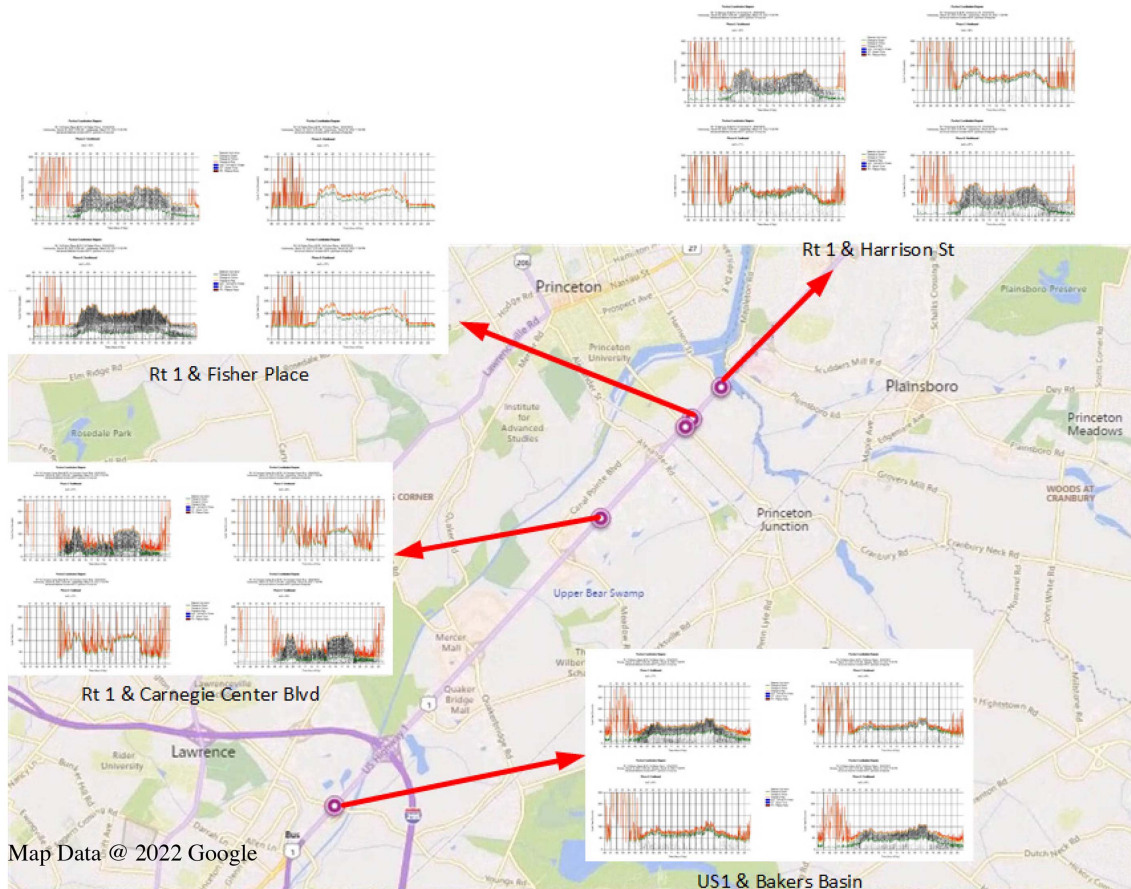


Fig. 17. Purdue coordination diagrams with algorithm reconstructed trajectory on different approaches from different locations. (Map data © 2022 Google.)

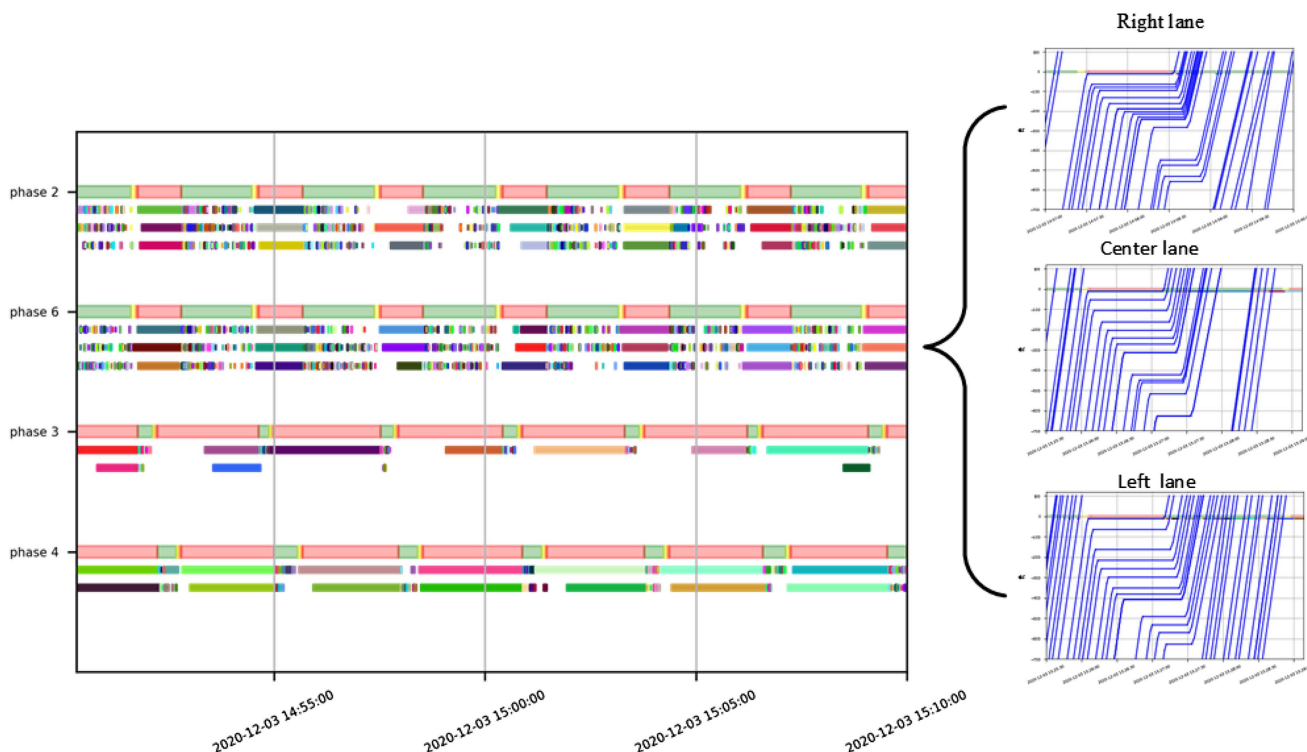


Fig. 18. Rutgers coordination diagram and time-space vehicle trajectory.

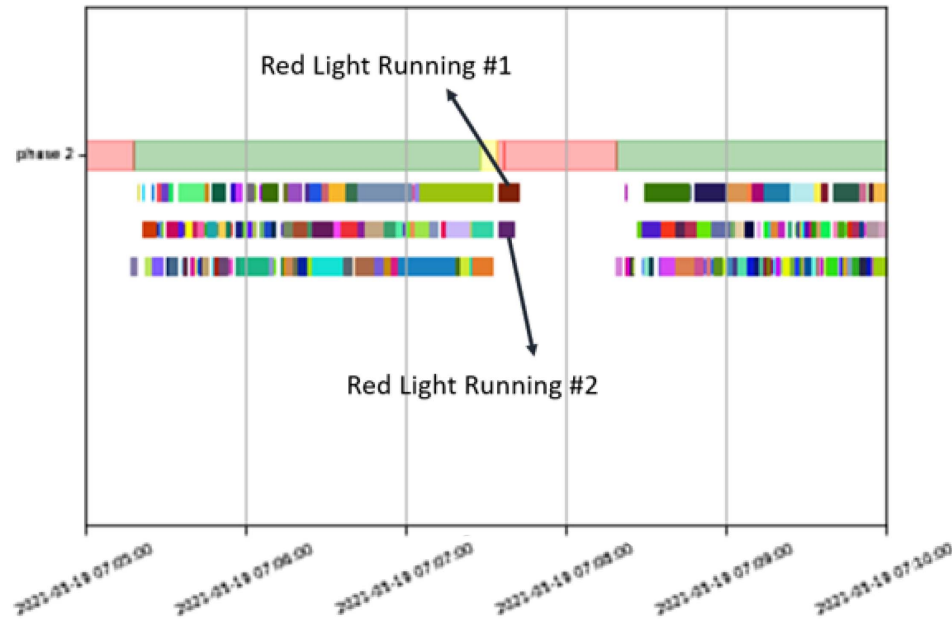


Fig. 19. Probable red light running captured by RCD.

Under the ideal condition, meaning the detector delay is negligible or can be adjusted with an offset, safety performance issues caused by signal timing can also be recognized from this RCD. For example, a probable red-light-running event can quickly be flagged when vehicles pass through the intersection during the red phase on the coordination diagram (Fig. 19). The two probable red-light-running events can be further investigated with Autoscope or CCTV video footage.

Conclusion and Future Work

This paper explored how to use the existing controller and detector systems to enable detector-data-dependent ATSPMs performance metrics without the need to upgrade the infrastructure. ATSPMs system are built on different types of detection input, whereas many signalized intersections often face data availability constraints due to the absence of the required detection system. This paper provides a solution to address the detector shortage problem using traffic flow theory and modeling. Because signal control systems are built on vehicle actuation detectors, most signal controllers are equipped with stopbar detectors. The proposed vehicle trajectory algorithm converts stopbar video sensors (e.g., Autoscope) into advanced detection events for ATSPMs. Using the trajectory reconstruction method from stopbar video detector to estimate advanced detector arrival information will save transportation agencies a substantial amount of investment to update their detection system to meet ATSPMs requirements.

Detection zone length is the main impacting factor of accuracy for stopbar detector, which is easy to calibrate. According to SCATS convention, a 15-ft presence was used as the default value. A novel traffic flow model was proposed to estimate shockwave queuing speed from stopbar occupancy. The queuing speed traffic flow model can be used for computing queue length and waiting for the delay that are used by adaptive signal control. As a byproduct, the Rutgers coordination diagram serves as a new visualization tool providing a pictorial description of how traffic signals serve the traffic demands lane-by-lane, which can be converted into a time-space diagram with vehicle trajectory data.

Future work to extend method includes the more extensive testing on the deployment corridors, investigating safety-related performance measurements using existing signal event and detector data. It is also understood that the integration of ATSPMs and adaptive signal control with connected vehicle (CV) technology will fundamentally change the information distribution and reshape future traffic control.

Appendix. Algorithm: Drawing Trajectory on STMap

```

Input: STMap, Turning points of trajectory
Outputs: Vehicle trajectory visualization on STMap
Known parameters:
FrameRate: frame/second
Scale-factor of each pixel: Scale (ft/pixel)
Video Start Time: Timestamp_video (0.1 s)
Stopbar row number on STMap: R_stopbar
For every detected vehicle
  For every turning point (Timestamp_tp, Distance_tp)
    Row_tp = Distance_tp/Scale + R_stopbar
    Col_tp = (Timestamp_tp-Timestamp_video)/FrameRate
    turning_pts.append([Col_tp, Row_tp])
  End For
  Connect all Turning_pts on STMap
End For

```

Data Availability Statement

Some or all data, models, or code that support the findings of this study are available from the corresponding author upon reasonable request.

Acknowledgments

The authors confirm their contribution to the paper as follows: study conception and design: Tianya Zhang, Peter Jin, Thomas Brennan, Kelly McVeigh, Mohammad Jalayer; data collection:

Kelly McVeigh, Thomas Brennan; analysis and interpretation of results: Tianya Zhang, Peter Jin, Thomas Brennan, Mohammad Jalayer, Deep Patel; draft manuscript preparation: Tianya Zhang, Peter Jin, Thomas Brennan, Mohammad Jalayer. All authors reviewed the results and approved the final version of the manuscript.

References

- Ardestani, S. M., P. J. Jin, and C. Feeley. 2016. "Signal timing detection based on spatial-temporal map generated from CCTV surveillance video." *Transp. Res. Rec.* 2594 (1): 138–147. <https://doi.org/10.3141/2594-17>.
- Cassidy, M. J. 1998. "Bivariate relations in nearly stationary highway traffic." *Transp. Res. Part B Methodol.* 32 (1): 49–59. [https://doi.org/10.1016/S0919-2615\(97\)00012-X](https://doi.org/10.1016/S0919-2615(97)00012-X).
- Chang, J., M. Talas, and S. Muthuswamy. 2013. "Simple methodology for estimating queue lengths at signalized intersections using detector data." *Transp. Res. Rec.* 2355 (1): 31–38. <https://doi.org/10.3141/2355-04>.
- Cheng, Y., X. Qin, J. Jin, B. Ran, and J. Anderson. 2011. "Cycle-by-cycle queue length estimation for signalized intersections using sampled trajectory data." *Transp. Res. Rec.* 2257 (1): 87–94. <https://doi.org/10.3141/2257-10>.
- Daganzo, C. F. 2005a. "A variational formulation of kinematic waves: Basic theory and complex boundary conditions." *Transp. Res. Part B Methodol.* 39 (2): 187–196. <https://doi.org/10.1016/j.trb.2004.04.003>.
- Daganzo, C. F. 2005b. "A variational formulation of kinematic waves: Solution methods." *Transp. Res. Part B Methodol.* 39 (10): 934–950. <https://doi.org/10.1016/j.trb.2004.05.003>.
- Day, C. M., D. M. Bullock, H. Li, S. M. Remias, A. M. Hainen, R. S. Freije, A. L. Stevens, J. R. Sturdevant, and T. M. Brennan. 2014. *Performance measures for traffic signal systems: An outcome-oriented approach*. Rep. No. TPF-5 (258). West Lafayette, IN: Purdue Univ. <https://doi.org/10.5703/128828431533>.
- Day, C. M., J. M. Ernst, T. M. Brennan Jr., C. S. Chou, A. M. Hainen, S. M. Remias, A. Nichols, B. D. Griggs, and D. M. Bullock. 2012. "Performance measures for adaptive signal control: Case study of system-in-the-loop simulation." *Transp. Res. Rec.* 2311 (1): 1–15. <https://doi.org/10.3141/2311-01>.
- Day, C. M., E. J. Smaglik, D. M. Bullock, and J. R. Sturdevant. 2008. *Real-time arterial traffic signal performance measures*. Publication FHWA/IN/JTRP-2008/09. West Lafayette, IN: Purdue Univ. <https://doi.org/10.5703/1288284313439>.
- Dixon, M., N. Jacobs, and R. Pless. 2009. "An efficient system for vehicle tracking in multi-camera networks." In *Proc., 2009 3rd ACM/IEEE Int. Conf. on Distributed Smart Cameras (ICDSC)*, 1–8. New York: IEEE.
- Emtenan, A. T., and C. M. Day. 2020. "Impact of detector configuration on performance measurement and signal operations." *Transp. Res. Rec.* 2674 (4): 300–313. <https://doi.org/10.1177/0361198120912244>.
- FHWA (Federal Highway Administration). 2021. "Intersection safety." Accessed April 11, 2022. <https://highways.dot.gov/research/research-programs/safety/intersection-safety>.
- Geroliminis, N., and A. Skabardonis. 2005. "Prediction of arrival profiles and queue lengths along signalized arterials by using a Markov decision process." *Transp. Res. Rec.* 1934 (1): 116–124. <https://doi.org/10.1177/0361198105193400112>.
- Greenberg, H. 1959. "An analysis of traffic flow." *Oper. Res.* 7 (1): 79–85. <https://doi.org/10.1287/opre.7.1.79>.
- Greenshields, B. D., J. R. Bibbins, W. S. Channing, and H. H. Miller. 1935. "A study of traffic capacity." In Vol. 1935 of *Highway research board proceedings*. Washington, DC: National Research Council (US), Highway Research Board.
- Hall, F. L. 1996. "Traffic stream characteristics." In *Traffic flow theory*, 36. Washington, DC: US Federal Highway Administration.
- Hall, F. L., and B. N. Persaud. 1989. *Evaluation of speed estimates made with single-detector data from freeway traffic management systems*. Washington, DC: Transportation Research Record.
- Hallenbeck, M. E., J. M. Ishimaru, K. D. Davis, and J. M. Kang. 2008. "Arterial performance monitoring using stop bar sensor data." In *Proc., 87th Annual Meeting of the Transportation Research Board*.
- Washington, DC: National Academies of Sciences, Engineering, and Medicine.
- Huang, T., S. Poddar, C. Aguilar, A. Sharma, E. Smaglik, S. Kothuri, and P. Koonce. 2018. "Building intelligence in automated traffic signal performance measures with advanced data analytics." *Transp. Res. Rec.* 2672 (18): 154–166. <https://doi.org/10.1177/0361198118791380>.
- Jin, P. J., T. Zhang, T. M. Brennan Jr., and M. Jalayer. 2019. *Real-time signal performance measurement (RT-SPM)*. Rep. No. FHWA NJ-2019-002. Washington, DC: USDOT, Federal Highway Administration.
- Kimley-Horn. 2019. "NCDOT automated traffic signal performance measures ATSPM implementation plan." Accessed May 11, 2022. <https://connect.ncdot.gov/resources/safety/Teppl/TEPPL%20All%20Documents%20Library/NCDOT%20ATSPM%20Implementation%20Plan.pdf>.
- Lighthill, M. J., and G. B. Whitham. 1955. "On kinematic waves II. A theory of traffic flow on long crowded roads." *Proc. R. Soc. London, Ser. A* 229 (1178): 317–345. <https://doi.org/10.1098/rspa.1955.0089>.
- Liu, H. X., X. Wu, W. Ma, and H. Hu. 2009. "Real-time queue length estimation for congested signalized intersections." *Transp. Res. Part C Emerging Technol.* 17 (4): 412–427. <https://doi.org/10.1016/j.trc.2009.02.003>.
- Malinovskiy, Y., Y. J. Wu, and Y. Wang. 2009. "Video-based vehicle detection and tracking using spatiotemporal maps." *Transp. Res. Rec.* 2121 (1): 81–89. <https://doi.org/10.3141/2121-09>.
- Manual, H. C. 2010. *HCM2010*, 1207. Washington, DC: Transportation Research Board, National Research Council.
- Moshiri, M., and J. Montufar. 2017. "Evaluation of detection sensitivity and count performance of advanced vehicle detection technologies at a signalized intersection." *J. Intell. Transp. Syst.* 21 (1): 52–62. <https://doi.org/10.1080/15472450.2016.1198700>.
- Mück, J. 2002. "Using detectors near the stop-line to estimate traffic flows." *Traffic Eng. Control* 43 (11): 429–434.
- Newell, G. F. 2002. "A simplified car-following theory: A lower order model." *Transp. Res. Part B Methodol.* 36 (3): 195–205. [https://doi.org/10.1016/S0919-2615\(00\)00044-8](https://doi.org/10.1016/S0919-2615(00)00044-8).
- Osorio, C., and C. Wang. 2017. "On the analytical approximation of joint aggregate queue-length distributions for traffic networks: A stationary finite capacity Markovian network approach." *Transp. Res. Part B Methodol.* 95 (Jan): 305–339. <https://doi.org/10.1016/j.trb.2016.07.013>.
- Remias, S., J. Waddell, M. Klawon, and K. Yang. 2018a. *Signal performance measures pilot implementation*. Rep. No. SPR-1681. Lansing, MI: Michigan DOT.
- Remias, S. M., C. M. Day, J. M. Waddell, J. N. Kirsch, and T. Trepanier. 2018b. "Evaluating the performance of coordinated signal timing: Comparison of common data types with automated vehicle location data." *Transp. Res. Rec.* 2672 (18): 128–142. <https://doi.org/10.1177/0361198118794546>.
- Rhodes, A., D. M. Bullock, J. Sturdevant, Z. Clark, and D. G. Candey Jr. 2005. "Evaluation of the accuracy of stop bar video vehicle detection at signalized intersections." *Transp. Res. Rec.* 1925 (1): 134–145. <https://doi.org/10.1177/0361198105192500114>.
- Sharma, A., D. M. Bullock, and J. A. Bonneson. 2007. "Input-output and hybrid techniques for real-time prediction of delay and maximum queue length at signalized intersections." *Transp. Res. Rec.* 2035 (1): 69–80. <https://doi.org/10.3141/2035-08>.
- Smaglik, E. J., C. Sobie, A. Sharma, C. Liu, and S. Kothuri. 2017. *Improving adaptive/responsive signal control performance: Implications of non-invasive detection and legacy timing practices*. Rep. No. FHWA-OR-RD-17-07. Salem, OR: Oregon DOT.
- Stevanovic, A. 2020. "Adaptive signal control systems and SPaT/connected vehicle applications." Accessed May 11, 2022. <https://www.fhwa.dot.gov/exit.cfm?link=https://connectdot.connectsolutions.com/pfn123jnbzyd/?launcher=false&fcsContent=true&pbMode=normal>.
- Sun, Z., and X. J. Ban. 2013. "Vehicle trajectory reconstruction for signalized intersections using mobile traffic sensors." *Transp. Res. Part C Emerging Technol.* 36 (Nov): 268–283. <https://doi.org/10.1016/j.trc.2013.09.002>.
- Taniguchi, H., T. Nakamura, and H. Furusawa. 1999. "Methods of traffic flow measurement using spatio-temporal image." In Vol. 4 of *Proc., 1999 Int. Conf. on Image Processing (Cat. 99CH36348)*, 16–20. New York: IEEE.

- Underwood, R. T. 1961. "Speed, volume and density relationships." In *Quality and theory of traffic flow*. New Haven, CT: Bureau of Highway Traffic, Yale Univ.
- Wang, X. B., X. Cao, and C. Wang. 2017. "Dynamic optimal real-time algorithm for signals (DORAS): Case of isolated roadway intersections." *Transp. Res. Part B Methodol.* 106 (Dec): 433–446. <https://doi.org/10.1016/j.trb.2017.06.005>.
- Wu, X., and H. X. Liu. 2011. "A shockwave profile model for traffic flow on congested urban arterials." *Transp. Res. Part B Methodol.* 45 (10): 1768–1786. <https://doi.org/10.1016/j.trb.2011.07.013>.
- Wu, X., H. X. Liu, and N. Geroliminis. 2011. "An empirical analysis on the arterial fundamental diagram." *Transp. Res. Part B Methodol.* 45 (1): 255–266. <https://doi.org/10.1016/j.trb.2010.06.003>.
- Zhang, T., and P. J. Jin. 2019. "A longitudinal scanline based vehicle trajectory reconstruction method for high-angle traffic video." *Transp. Res. Part C Emerging Technol.* 103 (Jun): 104–128. <https://doi.org/10.1016/j.trc.2019.03.015>.
- Zhang, T., P. J. Jin, Y. Ge, R. Moghe, and X. Jiang. 2022. "Vehicle detection and tracking for 511 traffic cameras with U-shaped dual attention inception neural networks and spatial-temporal map." *Transp. Res. Rec.* 2676 (5): 613–629. <https://doi.org/10.1177/03611981211068365>.
- Zhang, T. T., M. Guo, P. J. Jin, Y. Ge, and J. Gong. 2021a. "Longitudinal-scanline-based arterial traffic video analytics with coordinate transformation assisted by 3D infrastructure data." *Transp. Res. Rec.* 2675 (3): 338–357. <https://doi.org/10.1177/0361198120971257>.
- Zhang, T. T., P. J. Jin, T. M. Brennan Jr., K. McVeigh, and M. Jalayer. 2021b. *Automating the traffic signal performance measures for adaptive traffic signal control systems*. Rep. No. TRBAM-21-04207. Washington, DC: Transportation Research Board.